JGR Space Physics

RESEARCH ARTICLE
10.1029/2025JA034222

Midnight Simultaneous Observations of Spread-F and Multiple F-Layer Stratifications During the 11–12 May 2024 Geomagnetic Superstorm

P. R. Fagundes[1], V. G. Pillat[1], C. M. Anoruo[1], G. A. S. Picanço[1], M. Pezzopane[2], J. B. Habarulema[3,4,5], K. Venkatesh[6], A. Tardelli[1], A. L. Christovam[1], and F. Vieira[7]

[1]Laboratorio de Fısica e Astronomia, Universidade do Vale do Paraıba (UNIVAP), Urbanova, Brazil, [2]Istituto nazionale di geofisica e vulcanologia (INGV), Rome, Italy, [3]South African National Space Agency (SANSA), Hermanus, South Africa, [4]Department of Physics and Electronics, Rhodes University, Makhanda, South Africa, [5]Centre for Space Research, Physics Department, North-West University, Potchefstroom, South Africa, [6]Physical Research Laboratory (PRL), Ahmedabad, India, [7]Instituto Federal de Tocantins (IFTO), Observatório de Física Espacial, Araguatins, Brazil

Abstract A geomagnetic superstorm occurred from May 10 to 12, 2024, producing significant spatial and temporal disturbances in the ionosphere. Ground-based ionosonde and GPS-TEC data enabled the identification, analysis, and possible interpretation of a unique event: the simultaneous occurrence of Spread-F and multiple F-layer stratifications during the local midnight hours of May 11. To the best of our knowledge, this is the first documented case of such a phenomenon occurring at local midnight. This study provides new insights into the dynamics of the equatorial and low-latitude ionosphere under extreme geomagnetic conditions and highlights the critical role of coordinated, multi-instrument observations in advancing our understanding of ionospheric electrodynamics.

Plain Language Summary In May 2024, a powerful solar eruption, called a Coronal Mass Ejection, caused one of the strongest geomagnetic storms in the last 20 years. This storm had major effects on Earth's upper atmosphere, especially in a region called the ionosphere, which plays a key role in radio and GPS signals. Scientists used different tools, including GPS data and ground-based instruments, to study how the ionosphere reacted. On the night of 11 May they observed two simultaneous unusual features: disturbances known as Spread-F and a layered structure in the ionosphere, both occurring around midnight, something never reported before. Another type of F-layer stratification was also seen during the day on 12 May. These discoveries help scientists better understand how extreme solar activity can disturb our space environment and affect the technologies we rely on.

Key Points:

- First-ever observation of simultaneous Spread-F and multiple F-layer stratifications around midnight during a geomagnetic storm
- Improved understanding of equatorial ionospheric behavior during a superstorm and show the importance of using multiple instruments together
- This study analyzes the space-time variations of ionosonde measurements and GPS-based Vertical TEC (VTEC), Rate of TEC, and Rate of TEC Index data

Correspondence to:
P. R. Fagundes,
fagundes@univap.br

Citation:
Fagundes, P. R., Pillat, V. G., Anoruo, C. M., Picanço, G. A. S., Pezzopane, M., Habarulema, J. B., et al. (2025). Midnight simultaneous observations of spread-F and multiple F-layer stratifications during the 11–12 May 2024 geomagnetic superstorm. *Journal of Geophysical Research: Space Physics*, *130*, e2025JA034222. https://doi.org/10.1029/2025JA034222

Received 26 MAY 2025
Accepted 27 OCT 2025

Author Contributions:

Conceptualization: P. R. Fagundes
Data curation: P. R. Fagundes, V. G. Pillat, C. M. Anoruo, G. A. S. Picanço, M. Pezzopane, J. B. Habarulema, K. Venkatesh, A. Tardelli, A. L. Christovam, F. Vieira
Formal analysis: P. R. Fagundes, C. M. Anoruo, G. A. S. Picanço, K. Venkatesh, A. Tardelli, A. L. Christovam
Funding acquisition: P. R. Fagundes, F. Vieira
Investigation: P. R. Fagundes, V. G. Pillat, C. M. Anoruo, G. A. S. Picanço, M. Pezzopane, J. B. Habarulema, K. Venkatesh, A. Tardelli, A. L. Christovam, F. Vieira
Methodology: P. R. Fagundes, V. G. Pillat, C. M. Anoruo,

1. Introduction

Large-scale irregularities in the ionospheric F-layer are among the most extensively studied and intriguing phenomena in space weather research. Despite decades of investigation, many aspects of their generation and evolution remain not well understood and continue to be active areas of research (Booker & Wells, 1938; Patil et al., 2023). Typically, equatorial spread F (ESF) or large-scale ionospheric irregularities are nighttime phenomena strongly associated with the post-sunset electric field pre-reversal enhancement (PRE), which uplifts the F-layer and creates favorable conditions for their generation and development (e.g., Fagundes et al., 2009). In recent years, plasma bubbles and ionospheric irregularities on various spatial scales have been studied under both geomagnetically quiet and disturbed conditions. These studies have employed a combination of ground-based instruments, satellite observations, and numerical models (Alemu & Kassa, 2024; Buhari et al., 2017; De Michelis et al., 2021, 2022; Huba, 2023, 2024; Meng et al., 2018; Pi et al., 1997; Picanço et al., 2024; Sousasantos et al., 2025; Sripathi et al., 2011; Stolle et al., 2024; Wang et al., 2024; Zhao et al., 2025). Sahai et al. (2000) and Pimenta et al. (2001) highlighted the seasonal variation in the occurrence of plasma bubbles over the Brazilian sector, with higher activity observed from October to March and lower activity from April to September.

On the other hand, during the daytime, the ionosphere consistently exhibits the D, E, and F layers. The F-layer in the first hours of daytime splits into F1 and F2 layers, a process driven by plasma photo-production and recombination. At night, only the F2 layer remains, as the recombination process efficiently reduces plasma in the lower ionospheric regions, causing the D, E, and F1 layers to diminish significantly or disappear entirely.

G. A. S. Picanço, M. Pezzopane, J. B. Habarulema, K. Venkatesh
Project administration: P. R. Fagundes
Resources: P. R. Fagundes
Software: V. G. Pillat, G. A. S. Picanço, A. L. Christovam
Validation: P. R. Fagundes, V. G. Pillat, C. M. Anoruo, G. A. S. Picanço, M. Pezzopane, J. B. Habarulema, K. Venkatesh, A. Tardelli, A. L. Christovam, F. Vieira
Visualization: V. G. Pillat, M. Pezzopane, K. Venkatesh, A. Tardelli, A. L. Christovam
Writing – original draft: P. R. Fagundes
Writing – review & editing: V. G. Pillat, C. M. Anoruo, G. A. S. Picanço, M. Pezzopane, J. B. Habarulema, K. Venkatesh, A. Tardelli, A. L. Christovam, F. Vieira

However, during the morning-to-noon period, the F2 layer may undergo additional stratifications, leading to the formation of temporary F3 and even F4 layers, influenced by electrodynamic processes such as neutral winds, plasma diffusion, mesoscale traveling ionospheric disturbances (MSTIDs)/gravity waves (GWs), and upward ionospheric $E \times B$ drifts (Balan et al., 1998; Batista et al., 2002; Fagundes et al., 2007, 2011; Tardelli et al., 2016, 2018, 2022; Tardelli & Fagundes, 2015).

Several studies have investigated the occurrence of the F3-layer under quiet, storm, and superstorm conditions. According to Balan et al. (1998), the stratification of the F-layer into F2 and F3 components occurs during the morning to noon period in the equatorial region. This stratification is driven by a combination of $E \times B$ vertical drift and equatorward meridional neutral winds, which lifts the F-layer upward and creates favorable conditions for the formation of the F3-layer. On the other hand, Fagundes et al. (2007) suggested that in regions surrounding the equatorial ionization anomaly (EIA) crest at low latitudes, the formation of the F3-layer requires an additional mechanism. They proposed MSTIDs or GWs as likely candidates. More recently, Venkatesh and Patra (2022) investigated the formation of the F3-layer during the evening hours at Jicamarca (11.9°S, 282.7°E), attributing it to moderate plasma drift and a small or negligible height gradient in the vertical plasma drift.

In addition, Balan et al. (2008) examined the unusual formation of the F3-layer during the superstorm of November 2004. The F3-layer was observed in the afternoon (14:00–16:00 LT) and again in the evening (17:00–18:00 LT). They proposed that this unusual F3-layer formation could be driven by strong vertical $E \times B$ drifts associated with prompt penetration electric fields (PPEFs). Jin et al. (2021) studied the formation of the daytime F3-layer during the main and recovery phases of geomagnetic storms. They noted that the F3-layer was inhibited during the daytime in the recovery phase. Similarly, Sreeja et al. (2009) investigated the behavior of the F-layer under geomagnetically disturbed conditions associated with PPEFs, and emphasized the important role of electrodynamics in the redistribution of ionization, which can lead to the formation of the F3-layer. Venkatesh et al. (2019) using six simultaneous ionosonde data during the March 2015 superstorm, from the northern to the southern hemispheres, reported F3-layer appearances over a large latitudinal area but with some hemisphere asymmetries. In addition, they showed that the F3-layer at Boa Vista (BOAV, 2.8°N, 60.7°W) started at evening and extended to nighttime. These previous F3-layer research studies indicated that under disturbed conditions, the F-layer stratification can occur during the afternoon, evening, and night.

The May 2024 superstorm has already been studied by several researchers, including Astafyeva et al., 2025; Carmo et al., 2024; Evans et al., 2024; Fagundes et al., 2025; Guo et al., 2024; Jain et al., 2025; Karan et al., 2024; Lazzús & Salfate, 2024; Mlynczak et al., 2024; Nayak et al., 2025; Ranjan et al., 2024; Spogli et al., 2024. However, this investigation reports, for the first time, the occurrence of spread-F and multiple F-layer stratifications at local midnight, a phenomenon that has not been addressed in previous studies. We believe this work contributes to the understanding of the May 2024 superstorm by presenting and discussing a unique case of simultaneous observations of spread-F and multiple F-layer stratifications, specifically around midnight on 11 May. To the best of our knowledge, this is the first reported instance of the simultaneous occurrence of spread-F and multiple F-layer stratifications at local midnight.

2. Data Analysis

In Figure 1a, on 10 May at 17:00 Universal Time (UT), the solar wind velocity was approximately 400 km/s. It then suddenly increased to about 700 km/s and subsequently continued to rise gradually, reaching nearly 1,000 km/s by 12 May. Additionally, the Interplanetary Magnetic Field Bz (IMF Bz) was highly disturbed from 10 May at 17:00 UT to 11 May, showing strong oscillations between southward and northward orientations, although it remained predominantly southward during most of this interval. The SYM-H index displayed the characteristic temporal evolution of a geomagnetic storm (Figure 1c). The storm commencement occurred between 17:00 and 18:00 UT, when SYM-H peaked at 88 nT at 17:15 UT (highlighted by the yellow rectangle). It then starts the main phase (blue rectangle), rapidly decreasing until it reached its minimum value of −518 nT (Dst). Thereafter, the recovery phase began. To evaluate the role of the PPEF, the equatorial ionospheric eastward and westward electric fields during quiet time, as well as the combined quiet-time and disturbed prompt penetration electric field (PPEF), were computed at 48°W (Araguatins longitude: 48.1°W) using the Real-time Model of the Equatorial Ionospheric Electric Field (eastward electric field (EEF)–https://geomag.colorado.edu/online-calculators/real-time-model-ionospheric-electric-fields). As shown in Figure 1d, during the main phase and the

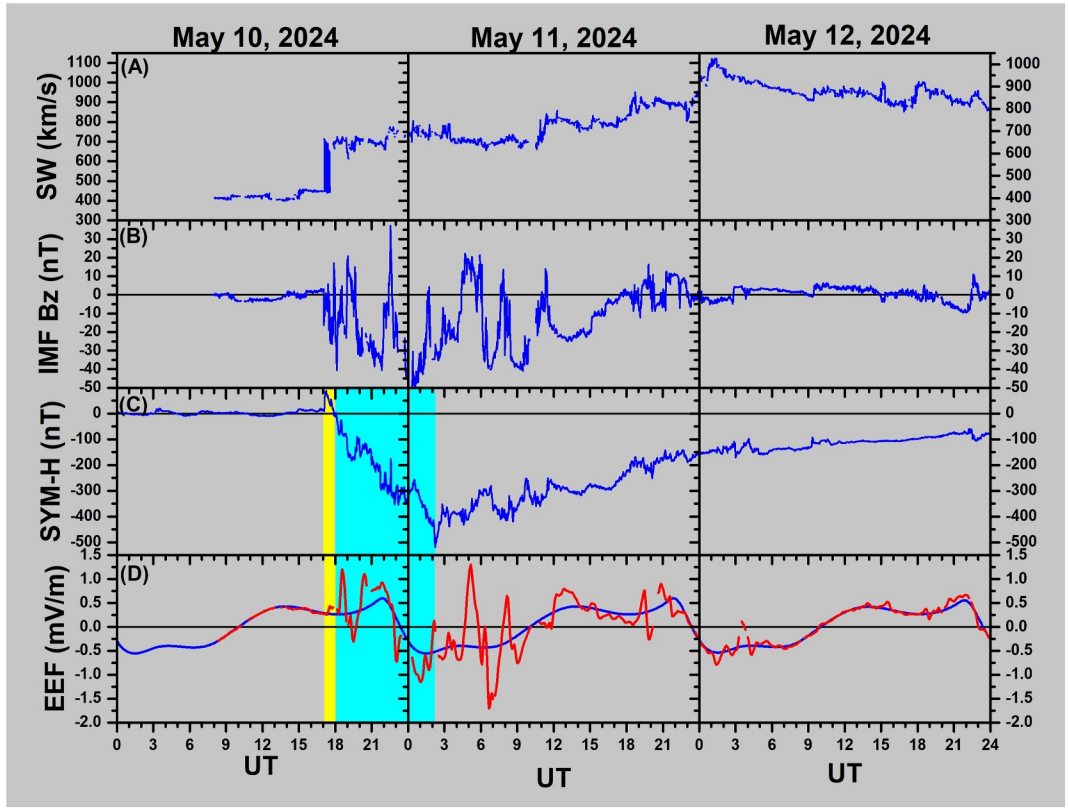

Figure 1. Observed temporal variations from 10 May to 12 May of the solar-interplanetary parameters, using data from GOES satellite data. (a) Solar wind (SW) speed (SW). (b) Interplanetary magnetic field Bz (IMF Bz). (c) SYM-H index. (d) The equatorial ionospheric eastward electric field is calculated at 48°W (https://geomag.colorado.edu/online-calculators/real-time-model-ionospheric-electric-fields). The sudden superstorm commencements and main phases are highlighted by yellow and blue rectangles, respectively.

first hour of the recovery phase, the PPEF oscillated multiple times between eastward and westward directions (Manoj et al., 2008; Manoj & Maus, 2012).

In this study, we analyze and discuss co-located ionosonde and GPS-TEC observations at Araguatins (ARA; 5.7°S, 48.1°W, dip-latitude −6.2°), a site located in the near-equatorial region, along with data from a network of 12 GPS-TEC stations. The Canadian Advanced Digital Ionosonde, employed in this investigation, operates in two simultaneous modes (Grant et al., 1995). In the first mode, it scans 150 frequencies every 300 s, producing standard ionograms with a temporal resolution of 5 min (Figures 2 and 3), which are commonly used for identifying F3-layer stratification. In the second mode, the ionosonde scans six fixed frequencies (3, 4, 5, 6, 7, and 8 MHz) at a higher temporal cadence of 100 s. Although this mode provides lower spectral resolution, it yields higher temporal resolution ionograms, allowing for detailed analysis of the virtual altitude of reflection (h′F) variations over time. The resulting figure, known as iso-frequency lines (Figures 4a and 4b), enable the investigation of rapid F-layer dynamics.

The Total Electron Content (TEC) and Vertical TEC (VTEC) are derived from a dual-frequency GPS receiver. As GPS signals cross the ionosphere, they experience a frequency-dependent delay. This delay can be analyzed to derive estimates of the TEC along the signal path.

This delay can be analyzed to derive estimates of TEC along the signal path. This is because the phase delay and the corresponding group delay advance are both proportional to the TEC crossed by the signal along the path (de Abreu et al., 2022; Pi et al., 1997). The TEC is measured in TEC units (TECu), where 1 TECu = 10^{16} electrons/m^2. Using the equations below, it is possible to infer TEC, VTEC, rate of change of TEC (ROT), and ROT index (ROTI).

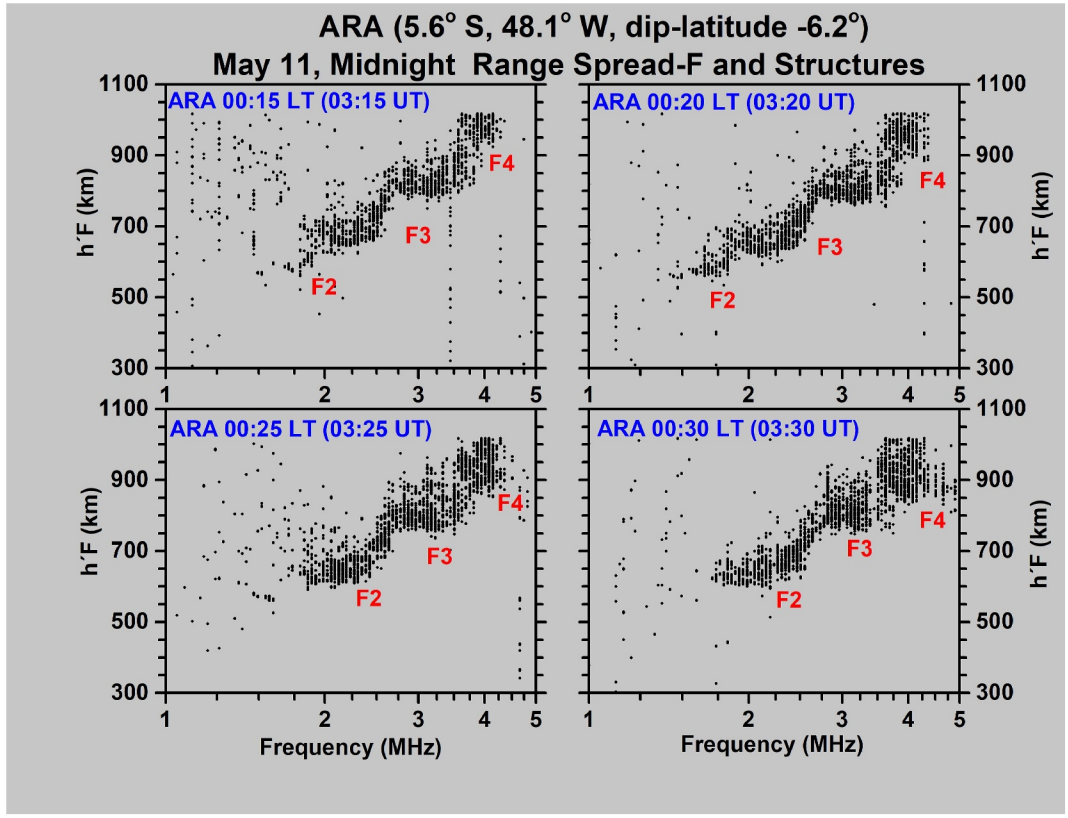

Figure 2. Ionograms recorded on 11 May 2024 at 00:15, 00:20, 00:25, and 00:30 Local Time (03:15, 03:20, 03:25, and 03:30 Universal Time), showing the presence of Spread-F and multiple F-layer stratifications such as the "F2," "F3," and "F4" layers.

For a dual-frequency GPS receiver, the ionospheric delay for a specialty frequency is given by

$$\Delta t = \frac{40.3\ \mathrm{TEC}}{f^2} \tag{1}$$

For dual frequencies (f_1 and f_2), the ionospheric delay difference can be expressed as

$$\Delta \varnothing = \frac{40.3\ \mathrm{TEC}}{f_1^2} - \frac{40.3\ \ \mathrm{TEC}}{f_2^2} \tag{2}$$

and consequently

$$\mathrm{TEC} = \frac{f_1^2\, f_2^2}{40.3\left(f_1^2 - f_2^2\right)}\left(\varnothing_1 - \varnothing_2\right) \tag{3}$$

where ϕ_1 and ϕ_2 are the carrier phases, and f_1 and f_2 are the transmission frequencies of the GPS satellite signals. To obtain VTEC, a geometric conversion is applied:

$$\mathrm{VTEC} = \mathrm{TEC}\left(1 - \frac{R_T^2\ \mathrm{Cos}^2\ (E)}{(R_T + h)^2}\right)^{-1/2} \tag{4}$$

where R_T is the Earth's radius (~6,371 km), E is the elevation angle of the GPS satellite, and h is the real height of the ionospheric layer (~350 km).

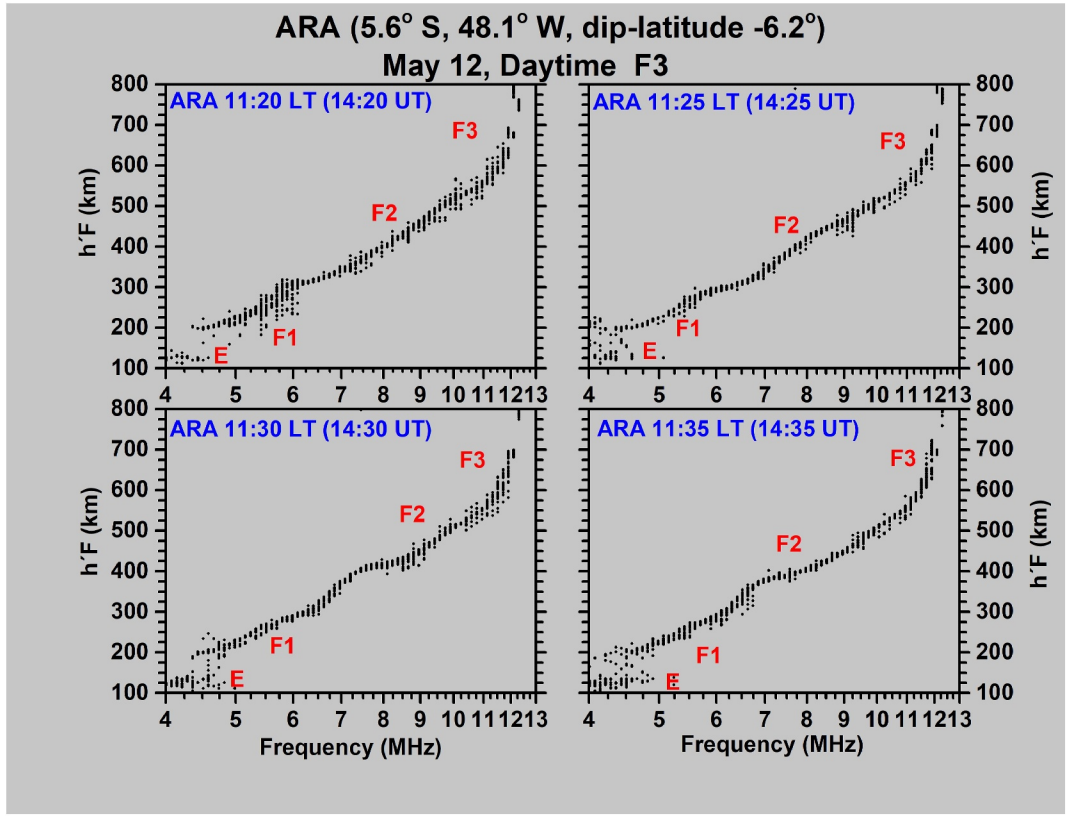

Figure 3. Ionograms recorded on 12 May 2024 at 11:20, 11:25, 11:30, and 11:35 Local Time (14:20, 14:25, 14:30, and 14:35 Universal Time), showing the presence of the E, F1, F2, and F3 layers.

Additionally, the ROT and the ROT Index (ROTI), defined as the standard deviation of ROT calculated over a 5-min interval, can be computed using the equations provided by Pi et al. (1997); ROT reflects phase fluctuations caused by ionospheric irregularities, while ROTI serves as a proxy for electron density fluctuations. A GPS-TEC network utilizing these two parameters is an effective tool for investigating large-to medium-scale ionospheric irregularities.

$$\mathrm{ROT} = \frac{\mathrm{VTEC}_{t+\Delta t} - \mathrm{VTEC}_{t}}{\Delta t} \tag{5}$$

$$\mathrm{ROTI} = \left(\left\langle \mathrm{ROT}^2 \right\rangle - \langle \mathrm{ROT} \rangle^2\right)^{1/2} \tag{6}$$

where $\mathrm{VTEC}_{t+\Delta t}$ and VTEC_{t} represents the VTEC in two consecutive time points (at $t + \Delta t$ and t), typically spaced 1 minute apart, $\left\langle \mathrm{ROT}^2 \right\rangle$, and $\langle \mathrm{ROT} \rangle$ refers to average.

3. Observations and Results

The ionospheric response to a superstorm, such as the May 2024 event investigated in the present study, is expected to exhibit several atypical behaviors when compared to quiet-time conditions. Consequently, examining the ionosphere under such extreme geomagnetic disturbances offers a valuable opportunity to investigate unusual electrodynamic processes that are not typically observed during quiet time or even during storms. Astafyeva et al. (2025), Carmo et al. (2024), and Fagundes et al. (2025) reported that during the May 2024 superstorm, the PPEFs and PRE were exceptionally intense, leading to a significant uplift of the F-layer (Figure 1d). Additionally, Huang et al. (2025) observed abnormal ionospheric variations over China, characterized by multiple peaks, wavelike structures, and strong PPEF signatures.

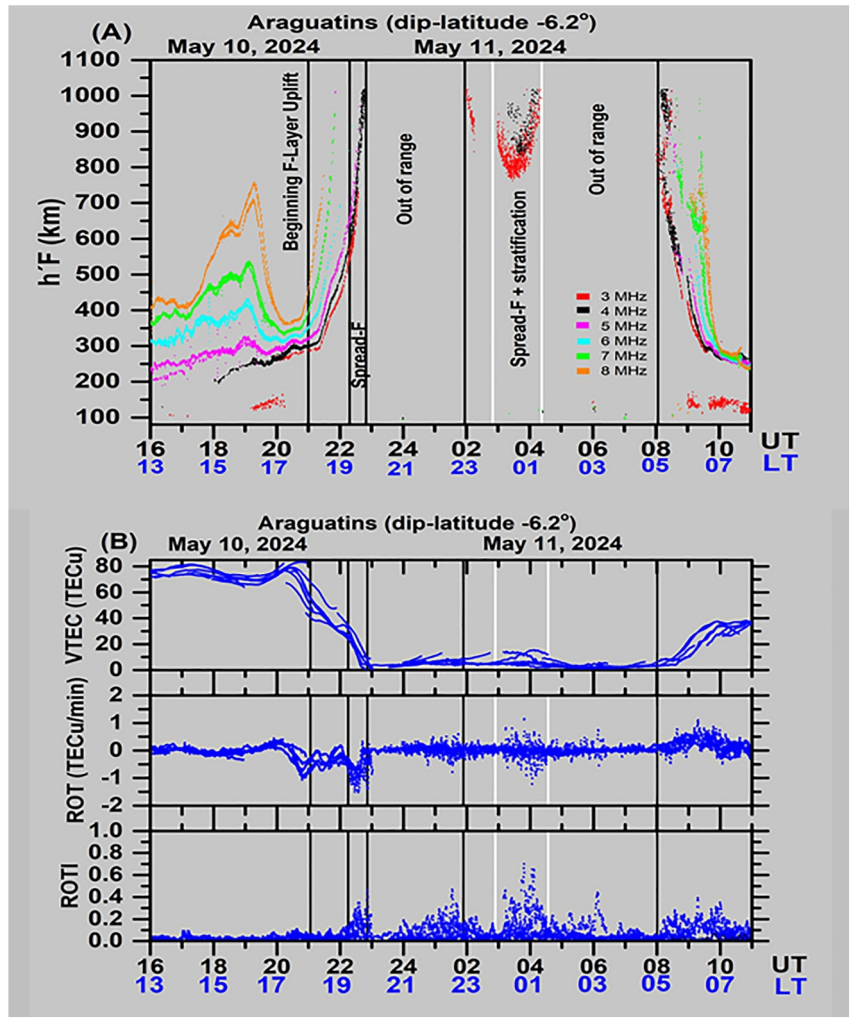

Figure 4. (a) Variations in virtual height (h'F) as a function of Universal Time (UT) and Local Time (LT) for fixed frequencies of 3, 4, 5, 6, 7, and 8 MHz, observed by the ionosonde at Araguatins (ARA), a station located near the magnetic equator, during the geomagnetic superstorm of May 10–11, 2024. The data cover the interval from 16:00 UT to 11:00 UT (corresponding to 13:00 LT to 08:00 LT). The vertical lines and labels indicate the different phases characterizing the F-layer, while the period between the white vertical lines marks the observation of spread-F and multiple F-layer stratification. (b) Same as (a) but for Vertical TEC, Rate of TEC, and Rate of TEC Index as measured by the GPS receiver co-located with the ionosonde.

The altitude of the F-layer exceeded the maximum observable altitude range (1,024 km) of the ionosonde at Araguatins in the Brazilian sector, which prevented visualizing any ionogram echoes, from both the F and even the E layers. To analyze these peculiar conditions, Fagundes et al. (2025) used VTEC data, which revealed that the EIA was displaced to midlatitudes and exhibited strong latitudinal and longitudinal asymmetries.

The present study investigates an unusual ionospheric behavior observed around local midnight between 10 and 11 May 2024, as illustrated by the four ionograms in Figure 2. During this period, a combination of high-altitude (>500 km) range spread-F and multiple F-layer stratifications was recorded. These stratified layers resembled the typical daytime F2, F3, and F4 layers, yet they appeared between 02:35 and 04:30 UT (23:35–01:30 LT), which corresponds to local midnight.

Additionally, during the daytime recovery phase on May 12, a weak F3 layer was observed at the ARA region, as shown in Figure 3. These four ionograms highlight the temporal evolution of the E, F1, F2, and F3 layers. It is important to note that F-layer stratification in the Brazilian sector typically occurs during daytime hours, between

08:00 and 14:00 LT (Fagundes et al., 2007, 2011; Tardelli et al., 2016, 2018, 2022; Tardelli & Fagundes, 2015), making the occurrence of such stratification around midnight particularly unusual.

When comparing daytime F-layer stratifications to the atypical multi-stratifications observed around midnight on 11 May, several key differences emerge. During the daytime, both the E layer and F1 layer are present due to strong photoionization driven by solar radiation. However, after sunset, these layers disappear quickly because electron and ion production ceases and the recombination processes prevail, particularly in the F1 layer, which is fast, with rates that depend on the square of the electron density. As a result, during nighttime, only the F2 layer typically remains, sustained by slower recombination rates and transport processes. In the unusual case discussed here, the F2 layer appears to undergo stratification processes, which give rise to additional F3 and F4 layers, a feature that is uncommon around local midnight.

Figure 4a illustrates that during the main phase of the superstorm, on May 10 at 21:00 UT (18:00 LT), the F-layer started uplifting from an initial height of 290 km. By 22:50 UT (19:50 LT), it had reached an altitude of 964 km, corresponding to an average uplift speed of approximately 368 km/hr. After this, typical F-layer traces were no longer recorded due to echoes being out of the ionosonde altitude range. This suggests that this rapid uplift of the F-layer was driven by a joint action of strong PPEF and electric field prereversal enhancement (PRE) effects (Carmo et al., 2024; Fagundes et al., 2025). On May 10, the quiet-time EEF (Figure 1d, blue line) exhibited a peak at approximately 22:00 UT (19:00 LT), which represents the PRE signature. In addition, the combined quiet-time and disturbed PPEF (Figure 1d, red line) shows a clear PPEF contribution superimposed on the PRE. When the altitude reached approximately 500 km at 22:20 UT (19:20 LT), spread-F was observed to begin. Notably, this occurred before the PPEF and PRE effects had completely ended. From 22:55 UT to 02:00 UT (19:55–23:00 LT), no ionograms were recorded, as the F-layer had risen beyond the maximum observable ionosonde altitude range (out of range). Following this, the ionosphere exhibited unexpected behavior as the F-layer began to descend. Surprisingly, during this period, a combination of spread-F and multiple F-layer stratifications ("F2," "F3," and "F4" layers) were recorded (Figure 2). These stratifications are similar to those typically recorded during daytime, but in this case were observed between 02:35 and 04:30 UT (23:35–01:30 LT), that is around local midnight. After 04:30 UT (01:30 LT), the ionosphere once again reached altitudes exceeding 1,024 km, making ionogram recordings empty. According to Huba (2023), significant advances have been made in spread-F modeling over the past decade. However, models applied to geomagnetic storms remain limited, as they often do not account for PPEF and disturbed dynamo fields. The observations discussed in this study highlight the importance of incorporating PPEF into models that simulate plasma bubble generation and spread-F during superstorms. Also, Huba (2023) pointed out that PRE plays a crucial role in ESF/plasma bubble onset.

Since a GPS-TEC receiver is co-located with the ionosonde installed at ARA, it is valuable to investigate the variations in VTEC, ROT, and ROTI during the 10–11 May superstorm. This complementary data set enhances our understanding of the formation and maintenance of ionospheric irregularities, particularly during periods when the F-layer height exceeded 1,024 km, rendering it out of range and consequently the ionogram trace was not visible. As shown by Fagundes et al. (2025), a strong negative ionospheric storm effect occurred at the ARA region during the main phase of the superstorm. Figure 4b illustrates that before 21:00 UT (18:00 LT), VTEC values ranged from approximately 70-85 TECu. However, within just two hours, these values dropped drastically to 5–10 TECu and remained at this low level until 11:00 UT (08:00 LT). This agreement between ionosonde and VTEC data reinforces the observed negative ionospheric response to the superstorm as observed by many studies (e.g., Aa et al., 2024; Carmo et al., 2024; Fagundes et al., 2025; Spogli et al., 2024; Themens et al., 2024).

This study presents the first-ever midnight observation of both Spread-F and multiple F-layer stratifications, marking a significant scientific finding. The observations suggest that a strong uplift of the F-layer during the evening elevated it to altitudes exceeding 1,000 km, creating conditions similar to those typically observed during daytime. This unusual uplift likely enabled the formation of F-layer stratifications during night. The vertical displacement of the F-layer appears to have redistributed the plasma into multiple layers, resembling the behavior of the daytime F3-layer. Notably, these multiple stratified layers were observed under very low electron density conditions, with TEC below 10 TECu and critical plasma frequencies less than 5 MHz (Figure 2). The multilayer structures became visible when the ionosphere descended to altitudes detectable by the ionosonde. Plasma uplift began around 21:00 UT, but ionosonde traces became invisible after 23:00 UT. While it is likely that the multilayer stratifications formed well before 03:00 UT, the absence of ionosonde data during that period limits our ability to confirm the exact timing.

The present results are consistent with those reported by Balan et al. (1998), who suggested that, in equatorial or near-equatorial regions, stratification is driven by a combination of $E \times B$ vertical drift and equatorward meridional neutral winds. These mechanisms contribute to the upward lifting of the F-layer during the daytime, thereby creating favorable conditions for the formation of the F3-layer.

During the May 2024 superstorm, the condition proposed by Balan et al. (1998) for F-layer stratification was exceptionally met at midnight, resulting in a rare event, the F-layer became stratified even during the occurrence of spread-F. It is important to note that although spread-F and multiple F-layer stratifications occurred simultaneously at midnight, they are independent phenomena. However, both are strongly associated with a significant uplift of the F-layer.

Huang et al. (2025) observed strong GW activity in the China sector during the May 2024 superstorm; however, their presence in the American sector is unlikely related to the formation of the F3-layer or the occurrence of spread-F. This interpretation is supported by Fagundes et al. (2007), who proposed that GWs and MSTIDs play a significant role in F3-layer formation only at low latitudes near the EIA crest. Additionally, Fagundes et al. (2009) showed that the post-sunset uplift of the F-layer is the primary driver of equatorial spread-F generation. In the present case, the combined effect of strong PRE and PPEF elevated the F-layer to very high altitudes after sunset, creating favorable conditions for the development of spread-F.

Between 22:20 UT (19:20 LT) and 22:50 UT (19:50 LT), ionosonde data indicate the presence of frequency spread-F, while ROT and ROTI data also suggest the occurrence of weak ionospheric irregularities, once again in agreement with ionosonde observations. From 22:55 UT (19:55 LT) to 02:00 UT (23:00 LT), ionosonde data were unavailable because the F-layer exceeded the observable altitude range. However, ROT and ROTI data continued to indicate the presence of weak to moderate ionospheric irregularities from 00:30 UT (21:30 LT) to 02:00 UT (23:00 LT). This suggests that, despite the ionosphere reaching altitudes beyond 1,024 km (out of range), irregularities of varying magnitudes persisted in the region. Notably, the strongest ROT and ROTI disturbances levels were observed precisely when spread-F and F-layer stratification occurred. This suggests that the combination of Spread-F and stratification increased the ROT and ROTI levels. After the occurrence of spread-F and stratification, the ROT and ROTI data remained at levels associated with the continued presence of Spread-F.

To highlight F-layer disturbances during the superstorm, Figure 5a presents iso-frequency lines during quiet conditions, for the days before the event (8–9 May 2024). At 22:00 UT (19:00 LT), the height was recorded at 245 km. Under the action of the PRE, the F-layer began to uplift, reaching 345 km by 01:35 UT, corresponding to an uplift speed of 27.9 km/hr, significantly lower than the one of 368 km/hr observed during the superstorm. Additionally, frequency spread-F was first observed at 00:35 UT (21:35 LT), evolving into mixed and range spread-F by 01:40 UT (22:40 LT), and persisted until 07:15 UT (04:15 LT). Frequency spread-F reappeared later, between 07:20 and 07:50 UT (04:20–04:50 LT). Notably, the maximum echoes during this period did not exceed 750 km and therefore remained within the ionosonde's maximum observable altitude range. In Figure 5b (quiet time), the same vertical ("*Y*-axis") scale is used as in Figure 4b (disturbed time) to maintain consistency. This allows for a direct comparison and emphasizes the intensity of the ROT and ROTI disturbances during the superstorm. Despite the presence of spread-F during the quiet period, no ROT or ROTI disturbances were noticed, highlighting how extreme the disturbances were during the event under study.

Furthermore, two GPS-TEC networks were employed to investigate the spatiotemporal features of the ionospheric irregularities. These networks are oriented along latitudinal and longitudinal directions, respectively. The configuration and locations of the GPS-TEC stations comprising these networks are presented in Figure 6 and Table 1.

The ROT and ROTI values for the chosen stations are shown in Figure 7 (with a latitudinal alignment) and 7 (with a longitudinal alignment), respectively. According to Sahai et al. (2007), when ROT phase fluctuations are observed exclusively at stations at the equatorial and near the equatorial region, the irregularity can be characterized as a bottomside irregularity event. In contrast, if these fluctuations extend from the equatorial region into low latitudes, the phenomenon is indicative of a large-scale ionospheric irregularity or plasma bubble. This classification approach is equally applicable to the interpretation of ROTI values.

Figures 7a and 7b show the ROT and ROTI values, respectively, for six GPS-TEC stations covering dip-latitudes from 15.1°N to 18.4°S (see Table 1 and Figure 6). This north–south (latitudinal) network is aligned with the ARA station, where simultaneous observations of spread-F and F-layer stratifications were recorded. Both ROT and

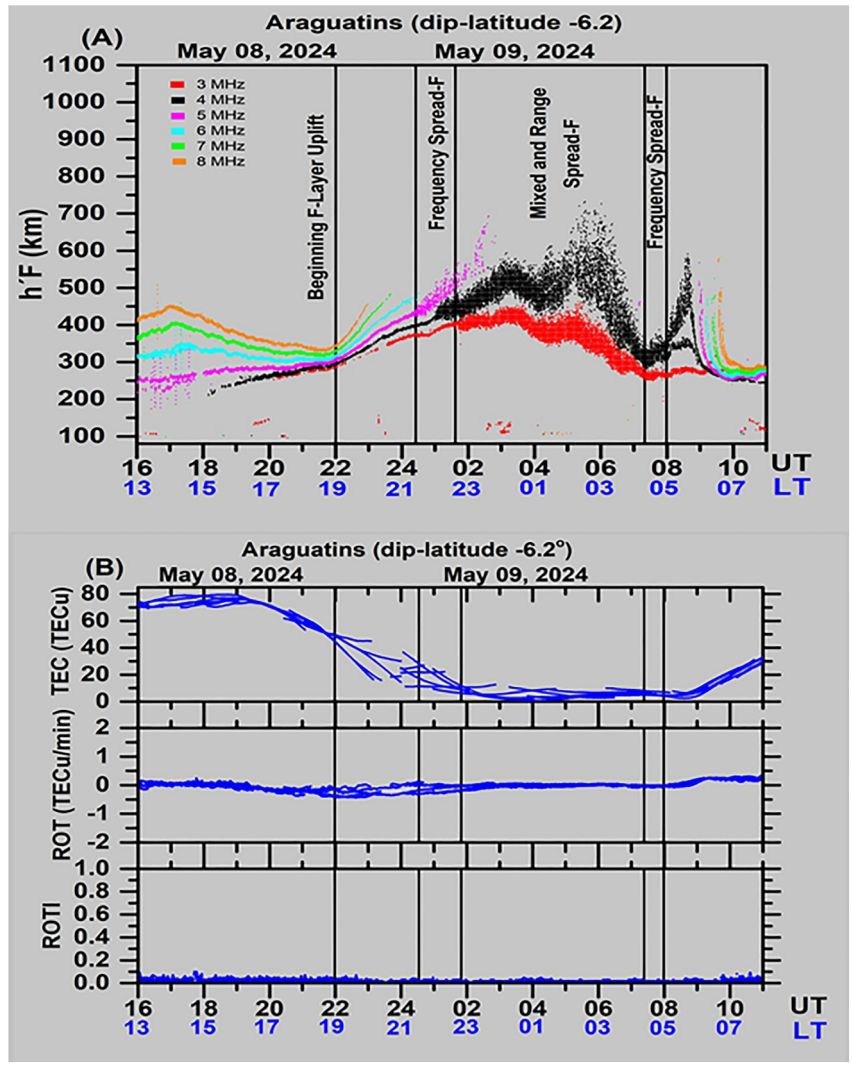

Figure 5. (a) Virtual height (h'F) variations as a function of Universal Time (UT) and Local Time (LT) for fixed frequencies at 3, 4, 5, 6, 7, and 8 MHz, observed at Araguatins (ARA, near the equatorial region) on 08–09 May 2024 (quiet time), from 15:00 UT to 11:00 UT (12:00 LT–08:00 LT). The vertical lines and labels indicate the different phases of the F-layer. (b) Same as (a) but for Vertical TEC, Rate of TEC, and Rate of TEC Index as measured by the GPS receiver co-located with the ionosonde.

ROTI indicate the presence of ionospheric irregularities of varying intensity from May 10 at 22:00 UT (19:00 LT) to May 11 at 10:00 UT (07:00 LT), spanning from the Northern to the Southern Hemisphere. These results suggest the development of large-scale ionospheric irregularities or plasma bubbles. Notably, the ROT and ROTI values are considerably more disturbed in the Southern Hemisphere, highlighting a clear latitudinal asymmetry of the ionospheric electrodynamic conditions. The white vertical lines indicate the period during which spread-F and F-layer stratifications were observed. It is important to mention that Carmo et al. (2024), using an all-sky imager at Cachoeira Paulista (Brazil, low latitude), observed the presence of an equatorial plasma bubble on 11 May. This observation reinforces that the GPS-TEC analysis (ROT and ROTI) presented in this study (Figure 7) accurately captured the large-scale ionospheric irregularity.

To verify whether ionospheric irregularities occurred simultaneously in both the western and eastern sectors, a network of six GPS-TEC stations was used (Figures 8a and 8b). Additionally, the longitudinal extent of this large-scale ionospheric irregularity was investigated. For this purpose, ROT and ROTI values from stations spanning longitudes from 69.9°W to 35.2°W were analyzed (see Table 1 and Figure 6). This longitudinally aligned GPS-TEC network crosses the ARA region, providing a basis for assessing the spatial development of the

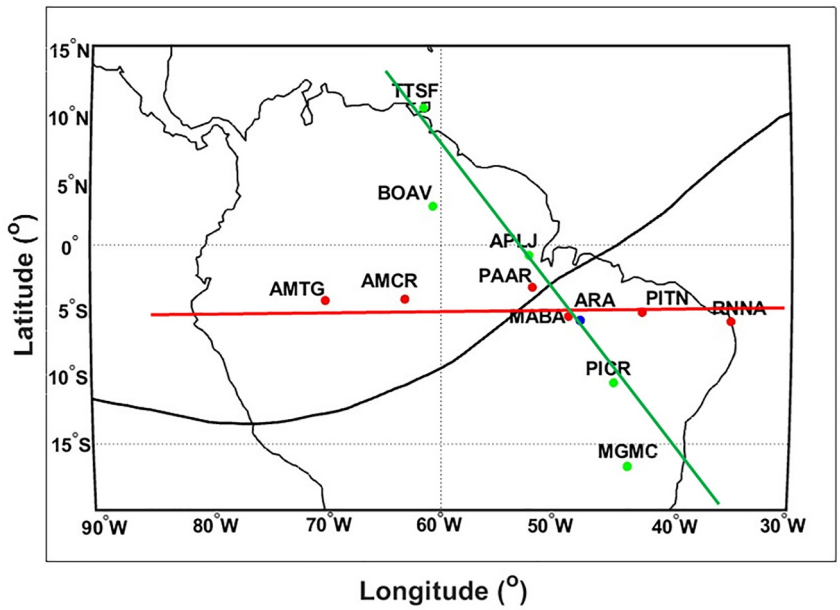

Figure 6. Map showing the locations of GPS-TEC stations forming the latitudinal (indicated by a green line and green dots) and longitudinal (indicated by a red line and red dots) networks over Brazil. The blue dot indicates the Araguatins (ARA) station, where the simultaneous appearance of spread-F and F-layer stratification is observed.

irregularities along the east–west direction. The results show no evidence of irregularities in the western sector (stations AMTG and AMCR), as the ROT and ROTI values at these locations do not exhibit typical signatures of ionospheric disturbances. At station PAAR, weak irregularity signatures are present but become more noticeable during the interval of observed spread-F and multiple F-layer stratifications. In contrast, stations MABA, PITN, and RNNA clearly display pronounced ROT and ROTI disturbances, indicating strong ionospheric irregularities in the eastern sector.

Table 1
Geographic Locations of GPS-TEC Station Codes, Geographic Latitude, Geographic Longitude, and Dip-Latitudes Over Brazil

Site	Latitude	Longitude	Dip-latitude
GPS-TEC latitude network: +North, +West, +North			
TTSF	10.3	61.5	15.1
BOAV	2.9	60.7	8.1
APLJ	−0.8	52.5	0.7
ARA	−5.7	48.1	−6.2
PICR	−10.4	45.2	−12.2
MGMC	−16.7	43.9	−18.4
GPS-TEC longitude network: +North, +West, +North			
AMTG	−4.2	69.9	5.1
AMCR	−4.1	63.1	2.9
PAAR	−3.2	52.2	−1.6
MABA	−5.4	49.1	−5.3
PITN	−5.1	42.8	−8.7
RNNA	−5.8	35.2	−13.7

4. Conclusion

The main objective of this investigation is to investigate the simultaneous midnight observations of spread-F and multiple F-layer stratifications during the transition from the main to the recovery phase, as well as the occurrence of daytime F-layer stratifications during the recovery phase of the May 2024 geomagnetic superstorm. This investigation utilizes ionosonde, VTEC, ROT, and ROTI data. Latitudinal and longitudinal GPS-TEC networks are used to study the spatiotemporal features of the ionospheric irregularities during the geomagnetic superstorm. The main conclusions of this investigation summarize as follows:

1. To the best of our knowledge, this is the first report of a simultaneous occurrence of spread-F and multiple F-layer stratifications during the midnight hours of a geomagnetic storm. This finding may encourage modelers to incorporate the effects of perturbed electric field penetration into spread-F and plasma bubble generation models.
2. During the main phase of the superstorm, the F-layer rose from an altitude of 290 km to an altitude of 964 km, which corresponds to an average uplift velocity of approximately 368 km/hr. In comparison, on the quiet day prior to the storm, the uplift velocity was only 27.9 km/hr.
3. This study suggests that a combination of PPEFs and PRE produced a highly significant uplift of the F-layer (see Figure 1d). This uplift pushed the layer well beyond the maximum observable altitude range of the

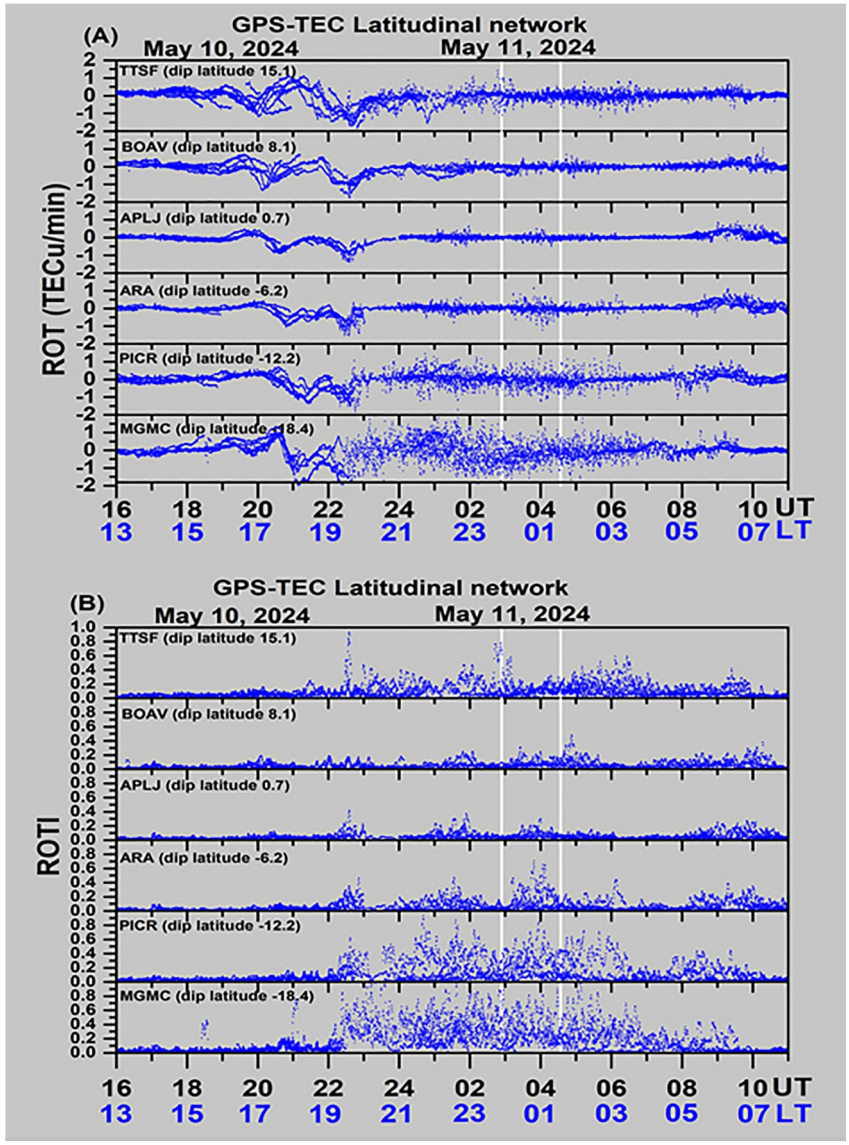

Figure 7. (a) Rate of TEC values for the TTSF, BOAV, APLJ, ARA, PICR, and MGMC stations, with a latitudinal alignment. (b) Same as (a), but showing Rate of TEC Index values.

ionosonde, which resulted in the absence of recorded echoes. This suggests that the strong uplift elevated the F-layer to heights above 1,000 km, creating during nighttime conditions similar to those typically observed during daytime, enabling the formation of F-layer stratifications.

4. On 12 May, during the recovery phase of the storm, the ionosonde at ARA detected the presence of E, F1, F2, and a weak F3 layer, indicating persistent and complex ionospheric structuring during daytime hours.
5. Data from the latitudinal GPS-TEC stations indicated the presence of a large-scale ionospheric irregularity or plasma bubble, which coincided with the occurrence of spread-F and multiple F-layer stratifications.
6. The longitudinal GPS-TEC network revealed that a large-scale irregularity or plasma bubble was present in the eastern sector of Brazil but absent in the western sector, suggesting a clear east–west asymmetry characterizing the storm-time ionospheric response.

These findings provide new insights into the behavior of the equatorial and low-latitude ionosphere during extreme geomagnetic disturbances and highlight the importance of simultaneous multi-instrument observations for an even-improving understanding of the ionospheric dynamics.

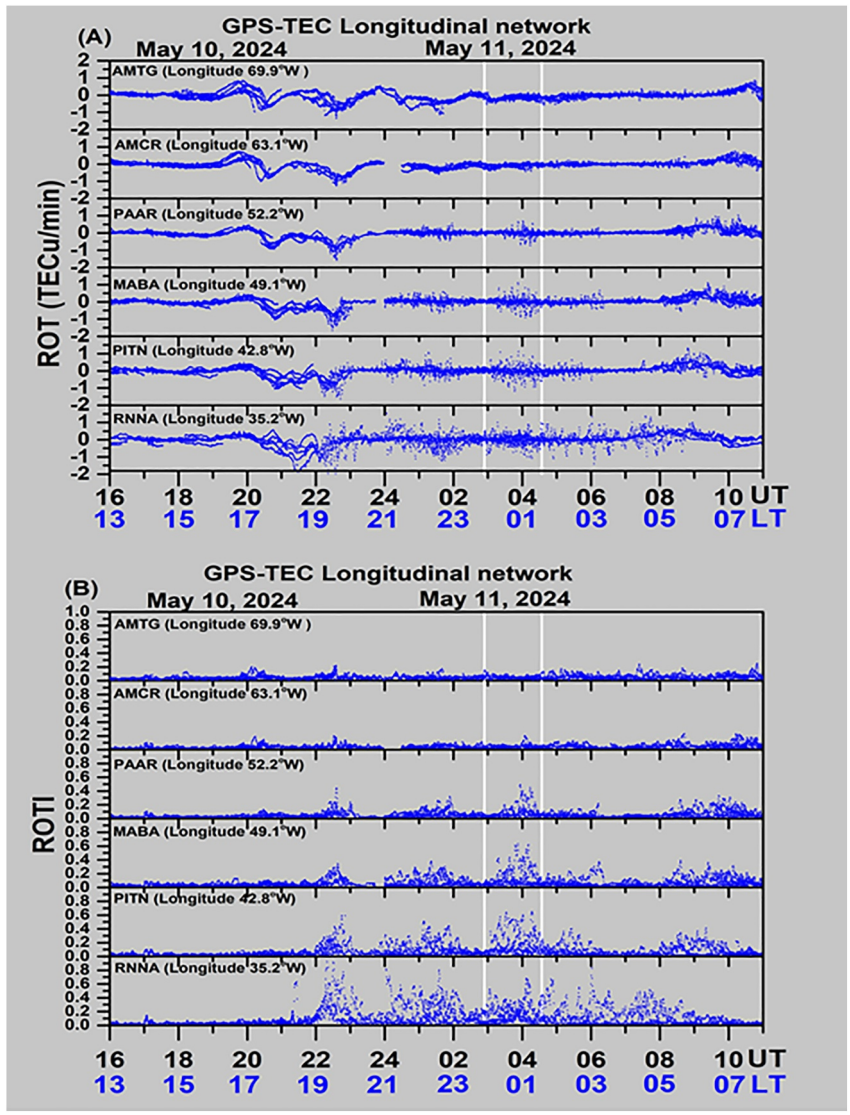

Figure 8. (a) Rate of TEC values for the AMTG, AMCR, PAAR, MABA, PITN, and RNNA stations with longitudinal alignment. (b) Same as (a), but showing Rate of TEC Index values.

Conflict of Interest

The authors declare no conflicts of interest relevant to this study.

Data Availability Statement

GPS data are available at IBGE and UNAVCO sites www.ibge.gov.br/en/home-eng.html?lang=en-GB and https://www.unavco.org/. Ionosonde and GPS data are available at Fagundes and Pillat, 2025; Fagundes and Pillat, 2025, respectively. Ionosonde data analysis is available at Pillat VG; Fagundes PR, 2025, and TEC data analysis is available at Pillat VG; Fagundes PR; de Oliveira AM, 2025. All paper data and software presented in this study are available for open access in the Zenodo repository at Fagundes (2025A, 2025B), Pillat and Fagundes (2025), and Pillat et al. (2025).

Acknowledgments
We would like to express our sincere thanks to the São Paulo Research Foundation (FAPESP) for the financial support under Grant 2022/14815-5. We would like to thank the National Council for Scientific and Technological Development (CNPq) for support through Grants 402724/2023-2 and 304721/2021-2, and the Brazilian Federal Agency for Support and Evaluation of Graduate Education (CAPES) for their support under Grant 88887.842761/2023-00. MP's contribution was partly by the Space It Up project funded by the Italian Space Agency, ASI, and the Ministry of University and Research, MUR, under contract No. 2024-5-E.0–CUP No. I53D24000060005. JBH's contribution was supported in part by the National Research Foundation of South Africa (Grants 116005 and 129285). KV's contribution was supported by the Department of Space, Government of India (Grant SRG/2023/001814). The Article Processing Charge for the publication of this research was funded by the Coordenação de Aperfeiçoamento de Pessoal de Nível Superior - Brasil (CAPES) (ROR identifier: 00x0ma614).

References

Aa, E., Zhang, S.-R., Lei, J., Huang, F., Erickson, P. J., Coster, A. J., et al. (2024). Significant midlatitude plasma density peaks and dual-hemisphere SED during the 10–11 May 2024 supergeomagnetic storm. *Journal of Geophysical Research: Space Physics*, *129*(11), e2024JA033360. https://doi.org/10.1029/2024JA033360

Alemu, Z., & Kassa, T. (2024). Investigation of equatorial plasma bubble irregularities under quiet and disturbed geomagnetic conditions over the East African longitudinal sector in 2015. *Advances in Space Research*, *75*(4), 3671–3691. https://doi.org/10.1016/j.asr.2024.12.012

Astafyeva, E., Maletckii, B., Förster, M., Ouar, I. D., Huba, J. D., Hairston, M. R., & Coley, W. R. (2025). Electrodynamic and ionospheric puzzles of the 10–11 May 2024 geomagnetic superstorm. *Journal of Geophysical Research: Space Physics*, *130*, e2024JA033284. https://doi.org/10.1029/2024JA033284

Balan, N., Batista, I. S., Abdu, M. A., MacDougall, J., & Bailey, G. J. (1998). Physical mechanism and statistics of occurrence of an additional layer in the equatorial ionosphere. *Journal of Geophysical Research*, *103*(A12), 29169–29181. https://doi.org/10.1029/98JA02823

Balan, N., Thampi, S. V., Lynn, K., Otsuka, Y., Alleyne, H., Watanabe, S., et al. (2008). F3 layer during penetration electric field. *Journal of Geophysical Research*, *113*(A3), A00A07. https://doi.org/10.1029/2008JA013206

Batista, I. S., Abdu, M. A., MacDougall, J., & Souza, J. R. (2002). Long term trends in the frequency of occurrence of the F3 layer over Fortaleza, Brazil. *Journal of Atmospheric and Terrestrial Physics*, *64*(12–14), 1409–1412. https://doi.org/10.1016/S1364-6826(02)00104-9

Booker, H. G., & Wells, H. W. (1938). Scattering of radio waves by the F-region of the ionosphere. *Terrestrial Magnetism and Atmospheric Electricity*, *43*(3), 249–256. https://doi.org/10.1029/TE043i003p00249

Buhari, S. M., Abdullah, M., Yokoyama, T., Otsuka, Y., Nishioka, M., Hasbi, A. M., et al. (2017). Climatology of successive equatorial plasma bubbles observed by GPS ROTI over Malaysia. *Journal of Geophysical Research: Space Physics*, *122*(2), 2174–2184. https://doi.org/10.1002/2016JA023202

Carmo, C. S., Dai, L., Wrasse, C. M., Barros, D., Takahashi, H., Figueiredo, C. A. O. B., et al. (2024). Ionospheric response to the extreme 2024 mother's daygeomagnetic storm over the Latin American sector. *Space Weather*, *22*(12), e2024SW004054. https://doi.org/10.1029/2024SW004054

De Michelis, P., Consolini, G., Alberti, T., Tozzi, R., Giannattasio, F., Coco, I., et al. (2022). Magnetic field and electron density scaling properties in the equatorial plasma bubbles. *Remote Sensing*, *14*(4), 918. https://doi.org/10.3390/rs14040918

de Abreu, A. J., Correia, E., Denardini, C. M., de Jesus, R., Venkatesh, K., Roberto, M., et al. (2022). Ionospheric GPS-TEC responses from equatorial region to the EIA crest in the South American sector under intense space weather conditions. *Journal of Atmospheric and Terrestrial Physics*, *227*, 105801. https://doi.org/10.1016/j.jastp.2021.105801

De Michelis, P., Consolini, G., Tozzi, R., Pignalberi, A., Pezzopane, M., Coco, I., et al. (2021). Ionospheric turbulence and the equatorial plasma density irregularities: Scaling features and RODI. *Remote Sensing*, *13*(4), 759. https://doi.org/10.3390/rs13040759

Evans, J. S., Correira, J., Lumpe, J. D., Eastes, R. W., Gan, Q., Laskar, F. I., et al. (2024). GOLD observations of the thermospheric response to the 10–12 May 2024 Gannon superstorm. *Geophysical Research Letters*, *51*(16), e2024GL110506. https://doi.org/10.1029/2024GL110506

Fagundes, P. R., Abalde, J. R., Bittencourt, J. A., Sahai, Y., Francisco, R. G., Pillat, V. G., & Lima, W. L. C. (2009). F layer postsunset height rise due to electric field prereversal enhancement: 2. Traveling planetary wave ionospheric disturbances and their role on the generation of equatorial spread F. *Journal of Geophysical Research*, *114*(A12), A12322. https://doi.org/10.1029/2009JA014482

Fagundes, P. R., Klausner, V., Bittencourt, J. A., Sahai, Y., & Abalde, J. R. (2011). Seasonal and solar cycle dependence of F3-layer near the southern crest of the equatorial ionospheric anomaly. *Advances in Space Research*, *48*(3), 472–477. https://doi.org/10.1016/j.asr.2011.04.003

Fagundes, P. R., Klausner, V., Sahai, Y., Pillat, V. G., Becker-Guedes, F., Bertoni, F. C. P., et al. (2007). Observations of daytime F2-layer stratification under the southern crest of the equatorial ionization anomaly region. *Journal of Geophysical Research*, *112*(A4), A04302. https://doi.org/10.1029/2006JA011888

Fagundes, P. R., & Pillat, V. G. (2025a). Midnight simultaneous observations of Spread-F and multiple F-Layer stratifications during the May 11-12, 2024 geomagnetic superstorm [dataset]. *Zenodo*. https://doi.org/10.5281/zenodo.15397899

Fagundes, P. R., & Pillat, V. G. (2025b). Midnight simultaneous observations of range Spread-F and multiple F-Layer stratifications during the May 11-12 geomagnetic superstorm (GPS_data). *Zenodo*. https://doi.org/10.5281/zenodo.16761649

Fagundes, P. R., Pillat, V. G., Habarulema, J. B., Muella, M. T. A. H., Venkatesh, K., de Abreu, A. J., et al. (2025). Equatorial Ionization anomaly disturbances (EIA) triggered by the May 2024 solar coronal mass ejection (CME): The strongest geomagnetic superstorm in the last two decades. *Advances in Space Research*. https://doi.org/10.1016/j.asr.2025.02.007

Grant, I. F., MacDougall, J. W., Ruohoniemi, J. M., Bristow, W. A., Sofko, G. J., Koehler, J. A., et al. (1995). Comparison of plasma flow velocities determined by the ionosonde doppler drift technique, SuperDARN radars, and patch motion. *Radio Science*, *30*(5), 1537–1549. https://doi.org/10.1029/95RS00831

Guo, X., Zhao, B., Yu, T., Hao, H., Sun, W., Wang, G., et al. (2024). East–west difference in the ionospheric response during the recovery phase of May 2024 super geomagnetic storm over the East Asian. *Journal of Geophysical Research: Space Physics*, *129*(9), e2024JA033170. https://doi.org/10.1029/2024JA033170

Huang, F., Lei, J., Yue, X., Li, Z., Zhang, N., Cai, Y., et al. (2025). Interplay of gravity waves and disturbance electric fields to the abnormal ionospheric variations during the 11 May 2024 superstorm. *AGU Advances*, *6*(1), e2024AV001379. https://doi.org/10.1029/2024AV001379

Huba, J. D. (2023). Resolution of the equatorial spread F problem: Revisited. *Front. Astron. Space Sci.*, *9*, 1098083. https://doi.org/10.3389/fspas.2022.1098083

Huba, J. D. (2024). Impact of meridional winds on the development of equatorial plasma bubbles: A review. *Front. Astron. Space Sci.*, *11*, 1472642. https://doi.org/10.3389/fspas.2024.1472642

Jain, A., Trivedi, R., Jain, S., & Choudhary, R. K. (2025). Effects of the super intense geomagnetic storm on 10-11 May, 2024 on total electron content at bhopal. *Advances in Space Research*, *75*(1), 953–965. https://doi.org/10.1016/j.asr.2024.09.029

Jin, Y., Zhao, B., Li, G., Li, Z., & Zhou, X. (2021). Inhibition of F3 layer at low latitude station Sanya during recovery phase of geomagnetic storms. *Journal of Geophysical Research: Space Physics*, *126*(12), e2021JA029850. https://doi.org/10.1029/2021JA029850

Karan, D. K., Martinis, C. R., Daniell, R. E., Eastes, R. W., Wang, W. B., McClintock, W. E., et al. (2024). GOLD observations of the merging of the Southern crest of the equatorial ionization anomaly and Aurora during the 10 and 11 May 2024 mother's day super geomagnetic storm. *Geophysical Research Letters*, *51*(15), e2024GL110632. https://doi.org/10.1029/2024GL110632

Lazzús, J. A., & Salfate, I. (2024). Report on the effects of the May 2024 Mother's day geomagnetic storm observed from Chile. *Journal of Atmospheric and Terrestrial Physics*, *261*, 106304. https://doi.org/10.1016/j.jastp.2024.106304

Manoj, C., & Maus, S. (2012). A real-time forecast service for the ionospheric equatorial zonal electric field. *Space Weather*, *10*(9), S09002. https://doi.org/10.1029/2012SW000825

Manoj, C., Maus, S., Luhr, H., & Alken, P. (2008). Penetration characteristics of the interplanetary electric field to the daytime equatorial ionosphere. *Journal of Geophysical Research*, *113*(A12), A12310. https://doi.org/10.1029/2008JA013381

Meng, X., Fang, H. X., Li, G. Z., & Weng, L. B. (2018). Statistical characteristics of locally generated ESF during equinoctial months over Sanya. *Advances in Space Research*, *61*(9), 2227–2233. https://doi.org/10.1016/j.asr.2017.11.040

Mlynczak, M. G., Hunt, L. A., Nowak, N., Marshall, B. T., & Mertens, C. J. (2024). Global thermospheric infrared response to the mother's day weekend extreme storm of 2024. *Geophysical Research Letters*, *51*(15), e2024GL110701. https://doi.org/10.1029/2024GL110701

Nayak, C., Buchert, S., Yiğit, E., Ankita, M., Singh, S., Tulasi Ram, S., & Dimri, A. P. (2025). Topside low-latitude ionospheric response to the 10–11 May 2024 super geomagnetic storm as observed by Swarm: The strongest storm-time super-fountain during the Swarm era? *Journal of Geophysical Research: Space Physics*, *130*(3), e2024JA033340. https://doi.org/10.1029/2024JA033340

Patil, A. S., Nade, D. P., Taori, A., Pawar, R. P., Pawar, S. M., Nikte, S. S., & Pawar, S. D. (2023). A brief review of equatorial plasma bubbles. *Space Science Reviews*, *219*, 1. https://doi.org/10.1007/s11214-023-00958-y

Pi, X., Mannucci, A. J., Lindqwister, U. J., & Ho, C. M. (1997). Monitoring of global ionospheric irregularities using the worldwide GPS network. *Geophysical Research Letters*, *24*(18), 2283–2286. https://doi.org/10.1029/97GL02273

Picanço, G. A. S., Denardini, C. M., Nogueira, P. A. B., Fagundes, P. R., Meza, A. M., Mendoza, L. P. O., et al. (2024). On the role of physical processes in controlling equatorial plasma bubble morphology. *Journal of Geophysical Research: Space Physics*, *129*(9), e2024JA032756. https://doi.org/10.1029/2024JA032756

Pillat, V. G., & Fagundes, P. R. (2025). UDIDA univap digital ionosonde data analysis, midnight simultaneous observations of Spread-F and multiple F-Layer stratifications during the May 11-12, 2024 geomagnetic superstorm [software]. *Zenodo*. https://doi.org/10.5281/zenodo.16740609

Pillat, V. G., Fagundes, P. R., & de Oliveira, A. M. (2025). UTECDA - Univap total electron content data analysis, midnight simultaneous observations of Spread-F and multiple F-Layer stratifications during the May 11-12, 2024 geomagnetic superstorm [software]. *Zenodo*. https://doi.org/10.5281/zenodo.16740647

Pimenta, A. A., Fagundes, P. R., Bittencourt, J. A., & Sahai, Y. (2001). Relevant aspects of equatorial plasma bubbles under different solar activity conditions. *Advances in Space Research*, *27*(6/7), 213–1218. https://doi.org/10.1016/S0273-1177(01)00200-9

Ranjan, A. K., Nailwal, D., Krishna, M. V. S., Kumar, A., & Sarkhel, S. (2024). Evidence of potential thermospheric overcooling during the May 2024 geomagnetic superstorm. *Journal of Geophysical Research: Space Physics*, *129*, e2024JA033148. https://doi.org/10.1029/2024JA033148

Sahai, Y., Becker-Guedes, F., Fagundes, P. R., Lima, W. L. C., Otsuka, Y., Huang, C. S., et al. (2007). Response of nighttime equatorial and low latitude F-region to the geomagnetic storm of August 18, 2003, in the Brazilian sector. *Advances in Space Research*, *39*(8), 1325–1334. https://doi.org/10.1016/j.asr.2007.02.064

Sahai, Y., Fagundes, P. R., & Bittencourt, J. A. (2000). Transequatorial F-region ionospheric plasma bubbles: Solar cycle effects. *Journal of Atmospheric and Terrestrial Physics*, *62*(5), 377–1383. https://doi.org/10.1016/S1364-6826(00)00179-6

Sousasantos, J., Rodrigues, F. S., Fejer, B. G., Eastes, R. W., & Moraes, A. O. (2025). Evidence of substorm-driven penetration electric field contributions to low-latitude phenomena: Enhanced upward drifts, plasma bubble development and severe scintillation. *Space Weather*, *23*(3), e2024SW004297. https://doi.org/10.1029/2024SW004297

Spogli, L., Alberti, T., Bagiacchi, P., Cafarella, L., Cesaroni, C., Cianchini, G., et al. (2024). The effects of the May 2024 mother's day superstorm over the mediterranean sector: From data to public communication. *Annals of Geophysics*, *67*(2), PA218. https://doi.org/10.4401/ag-9117

Sreeja, V., Devasia, C. V., Ravindran, S., Pant, T. K., & Sridharan, R. (2009). Response of the equatorial and low-latitude ionosphere in the Indian sector to the geomagnetic storms of January 2005. *Journal of Geophysical Research*, *114*(A6), A06314. https://doi.org/10.1029/2009JA014179

Sripathi, S., Kakad, B., & Bhattacharyya, A. (2011). Study of equinoctial asymmetry in the equatorial spread F (ESF) irregularities over Indian region using multi-instrument observations in the descending phase of solar cycle 23. *Journal of Geophysical Research*, *116*(A11), A11302. https://doi.org/10.1029/2011JA016625

Stolle, C., Siddiqui, T. A., Schreiter, L., Das, S. K., Rusch, I., Rother, M., & Doornbos, E. (2024). An empirical model of the occurrence rate of low latitude post-sunset plasma irregularities derived from CHAMP and swarm magnetic observations. *space weather-the international journal of research and applications*, *22*(6), e2023SW003809. https://doi.org/10.1029/2023sw003809

Tardelli, A., & Fagundes, P. R. (2015). Observations of ionospheric F layer quadruple stratification near equatorial region. *Journal of Geophysical Research: Space Physics*, *120*(1), 834–840. https://doi.org/10.1002/2014JA020653

Tardelli, A., Fagundes, P. R., Pezzopane, M., & Pillat, V. G. (2022). Longitudinal variations of the occurrence of F3 and F4 layers within the southern EIA and their dependence on solar cycle. *Advances in Space Research*, *69*(1), 59–70. https://doi.org/10.1016/j.asr.2021.08.011

Tardelli, A., Fagundes, P. R., Pezzopane, M., Venkatesh, K., & Pillat, V. G. (2016). Seasonal and solar activity variations of F3 layer and quadruple stratification (StF-4) near the equatorial region. *Journal of Geophysical Research: Space Physics*, *121*(12), 12116–12125. https://doi.org/10.1002/2016JA023580

Tardelli, A., Pezzopane, M., Fagundes, P. R., Venkatesh, K., Pillat, V. G., Cabrera, M. A., & Ezquer, R. G. (2018). Study of the F3 and StF4 layers at Tucumán near the southern crest of the equatorial ionization anomaly in western South America. *Journal of Geophysical Research: Space Physics*, *123*, 2156–2216. https://doi.org/10.1002/2017JA024539

Themens, D. R., Elvidge, S., McCaffrey, A., Jayachandran, P. T., Coster, A., Varney, R. H., et al. (2024). The high latitude ionospheric response to the major May 2024 geomagnetic storm: A synoptic view. *Geophysical Research Letters*, *51*(19), e2024GL111677. https://doi.org/10.1029/2024GL111677

Venkatesh, K., & Patra, A. K. (2022). Formation of the evening time F3 layer investigated using jicamarca incoherent scatter radar observations. *Journal of Geophysical Research: Space Physics*, *127*(2), e2021JA029684. https://doi.org/10.1029/2021JA029684

Venkatesh, K., Patra, A. K., Balan, N., Fagundes, P. R., Tulasi Ram, S., Batista, I. S., & Reinisch, B. W. (2019). Superfountain effect linked with 17 March 2015 geomagnetic storm manifesting distinct F3 layer. *Journal of Geophysical Research: Space Physics*, *124*(7), 6127–6137. https://doi.org/10.1029/2019JA026721

Wang, Z. H., Zou, S. S., Huba, J. D., & Ridley, A. (2024). Development of super plasma bubbles during the 7 September 2017 geomagnetic storm revealed by coupled GITM-SAMI3 simulations. *Geophysical Research Letters*, *51*, 22. https://doi.org/10.1029/2024GL112211

Zhao, X. K., Li, G. Z., Xie, H. Y., Hu, L. H., Sun, W. J., Li, Y., et al. (2025). A novel short-term prediction model for regional equatorial plasma bubble irregularities in east and Southeast Asia. *space weather-the international journal of research and applications*, *23*, 2. https://doi.org/10.1029/2024SW004224